Journal of Non-Crystalline Solids 627 (2024) 122801

Contents lists available at ScienceDirect

Journal of Non-Crystalline Solids

journal homepage: www.elsevier.com/locate/jnoncrysol

Topology of anisotropic glasses from persistent homology analysis

Zhiwen Pan [a], Achraf Atila [b], Erik Bitzek [c], Lothar Wondraczek [a,d,*]

[a] Otto Schott Institute of Materials Research, University of Jena, 07743 Jena, Germany
[b] Department of Materials Science and Engineering, Saarland University, 66123 Saarbrücken, Germany
[c] Max-Planck-Institut für Eisenforschung GmbH, Max-Planck-Str. 1, 40237 Düsseldorf, Germany
[d] Center of Energy and Environmental Chemistry, University of Jena, 07743 Jena, Germany

ARTICLE INFO

Keywords:
Glass
Anisotropy
Strain
Persistent homology
Silicate

ABSTRACT

Glasses are typically isotropic, but permanent or transient anisotropy can be induced by tensile strain. We use persistent homology (PH) analysis to explore the topological effects of such anisotropy in SiO_2—Na_2O glass ensembles with variable alkali concentration as a function of frozen-in anisotropic strain. Statistical information was extracted on ring (H_1) and cavity (H_2) features, whereby anisotropic stretching was found to induce strong variations in the ring topology of the –O-Si-O- backbone, but only minor changes in the overall cavity statistics or in the Na distribution (the Na distribution was found to be governed by H_2 persistence). Tensile fracture led to total recovery of network topology relative to the pristine (isotropic) glass. In revealing such reactions, PH and persistence similarity analysis may help to differentiate purely entropic orientation and irreversible structural alterations leading to glass anisotropy.

1. Introduction

The structure of disordered materials is challenging to describe due to the absence of long-range periodicity. Quantitative analyses are typically focusing on short- or intermediate-range structural motifs, such as interatomic bonds, polyhedral units, and rings of polyhedra [1–4]. Alternatively, global topological parameters have been proposed for structure-property correlations [5–9]. Various techniques are available to extract such parameters from glass datasets, from the counting of topological constraints based on short-range structural information [10] to persistent homology (PH) analysis of large representations of glass structure (for example, obtained through atomistic simulation) [11], or multivariate mining of composition-structure-property datasets [12]. The appeal of constraint counting lies in its simplicity: first-view considerations of cation coordination and interconnectivity allow for surprisingly powerful, semi-empirical predictions of macroscopic material properties such as hardness, glass transformation temperature, or even transport phenomena. On the other hand, the method does not truly reflect glassy disorder or non-affinity [13,14] and, *e.g.*, the interplay of variable states of bonding from ionic to covalent [15–17].

In contrast, PH is a mathematical tool that extracts topological features from network analysis [18,19]. Its primary feature are persistence diagrams (PDs), which describe the metric birth and death of homologous classes (simplexes) in a simplicial complex (Fig. 1**a**). PH has been applied to study the structure of glasses, whereby the constituting atoms are considered as interconnected nodes, and their positions in metric space are used as the simplicial complex. However, the physical interpretation of PDs of glass ensembles is challenging [11,20–23]. In particular, it is not possible to infer the structure of a unique simplex from individual birth-death datapoints due to high degeneracy: a single point in the PD could originate from a multitude of geometrically different structures. On the other hand, statistical analysis of PDs has been demonstrated *in principle* to enable global insights at intermediate-range structural features [24].

Here, we consider the applicability of PH analysis in the study of glasses exhibiting structural anisotropy. This case is unusual in two regards. For one, there is no anisotropy in topology *per se*. Secondly, glasses are usually isotropic materials, but transient or permanent structural anisotropy can be generated by post-processing. For example, uniaxial strain [25] above the glass transition temperature T_g, and subsequent cooling under load lead to a permanently anisotropic glass. This observation has been related to structural alignment, also reflected in non-Newtonian flow [26]; it is well-known for phosphate [26–28], silicate [29], and chalcogenide melts [30,31]. A very practical consequence is frozen-in or transient birefringence, used for (residual) stress analysis [32]. Aside from its phenomenology, however, the structural details of glass anisotropy remain unclear, for example, between purely entropic orientation or irreversible structural alterations. In this case,

* Corresponding author.

https://doi.org/10.1016/j.jnoncrysol.2023.122801
Received 22 August 2023; Received in revised form 21 December 2023; Accepted 21 December 2023
Available online 6 January 2024

PH analysis could provide additional information, whereby, for example, entropic stretching (and recovery) would not affect the extracted PDs, but irreversible effects should also reflect on the PD.

In vitreous silica, the statistics and directional preference of bond-switching reactions during loading and unloading lead to the orientation of the tetrahedral building units [33], but global topological changes are not known. On the other hand, the question as to whether structurally anisotropic glasses are topologically different from their isotropic analogues could not only contribute to a more complete picture of glass anisotropy and its macroscopic consequences. It could also help to understand transient material reactions during mechanical loading or thermal relaxation, the presence or absence of rubber elasticity, entropic relaxation and memory effects, and the role of permanent bond switching reactions and irreversible deformation [34].

In order to address this question, we apply PH and cavity scale analysis on isotropic and anisotropic sodium silicate glasses produced by molecular dynamic (MD) simulation. For this, we conduct similarity analyses on the full PD in terms of variations in global glass structure as a function of chemical composition and generated anisotropy; thereby, we avoid analyzing individual features on the PD. First, we identify the composition-dependence of global topological features in $(Na_2O)_y$-$(SiO_2)_{1-y}$ glasses. Subsequently, we explore delicate topological changes induced by uniaxial stretching. In addition to generating graphs that include all atoms, we conducted PH analysis on filtered graphs that include only the positions of Si atoms and Na atoms, respectively. While the Si graph represents the network backbone constructed from SiO4 tetrahedra, the Na graph indicates the presence of percolating network channels [35–38]. When considering Na topology, PH indicates how the Na ion network responds to strain, particularly at higher Na concentrations, leading to non-random topological adjustment.

2. Methods

2.1. Persistent homology

Persistent homology was computed using HomCloud (3.6.0) [39,40]. For input, we used the point coordinates of atoms in MD models of vitreous silica and sodium silicate glasses with variable sodium content and degrees of anisotropy (see the following section). Persistence diagrams were obtained for the full set of atoms as well as for the individual Si and Na sub-sets, for one and two-dimensional simplices (denoted H_1 and H_2, respectively; the index $n = \{1; 2\}$ is the Betti number corresponding to the number of individual cycles in topological space). H_2 reflects cavity units as defined in PH graph analyses [20,41], using the atom positions as graph nodes. An example of representing the initial glass structure as such a graph, together with its associated PD, is shown in Fig. 1**a**. The PD is a 2D histogram of the birth and death of complex simplices corresponding to the glass graph. The birth-death data are produced as follows: The initial atom positions (nodes) mark the birth of 0-dimensional (H_0) complex simplices, *i.e.*, points with a size of zero (**panel I in** Fig. 1**a**). Then, a filter is applied simultaneously on all nodes by growing their radius (**panel II in** Fig. 1**a**). Bonds are formed once any pair of nodes grown in this way generates a contact point (green sticks, **panel III in** Fig. 1**a**). At this stage, a part of H_0 dies. If a loop or a ring is formed by the bonds, a 1-dimensional simplex (H_1) is born. The H_1 simplex dies when its nodes grow to close a ring or loop (red stick, **panel IV in** Fig. 1**a**). Simplices with higher dimensionality (H_2, inset of Fig. 1**b**) are born upon the formation of a closed surface or cavity. Fig. 2**a** shows various H_2 simplices (marked in different colors) as the fundamental network units; they occupy almost the entire volume of the glass ensemble.

2.2. Glass preparation

To compare the topology of isotropic and anisotropic silicate glasses, we prepared a series of sodium silicate glasses with varying sodium content ($(Na_2O)_y$-$(SiO_2)_{1-y}$, $y = 0, 0.05, 0.1, 0.15, 0.2$) using classical molecular dynamics simulations. All MD simulations were carried out using the LAMMPS code [42]. The interactions between atoms were modeled using a potential developed by *Pedone* et al. [43]. This potential model was successfully used to simulate the mechanical properties of several oxide glasses [43–49]. The potential parameters and partial charges are provided in Ref. [43]. The short-range interaction cutoff was set to 5.5 Å, while long-range Coulomb interactions were treated using the damped shifted force method [50] with a cutoff of 8.0 Å and a damping parameter of 0.25 $Å^{-1}$.

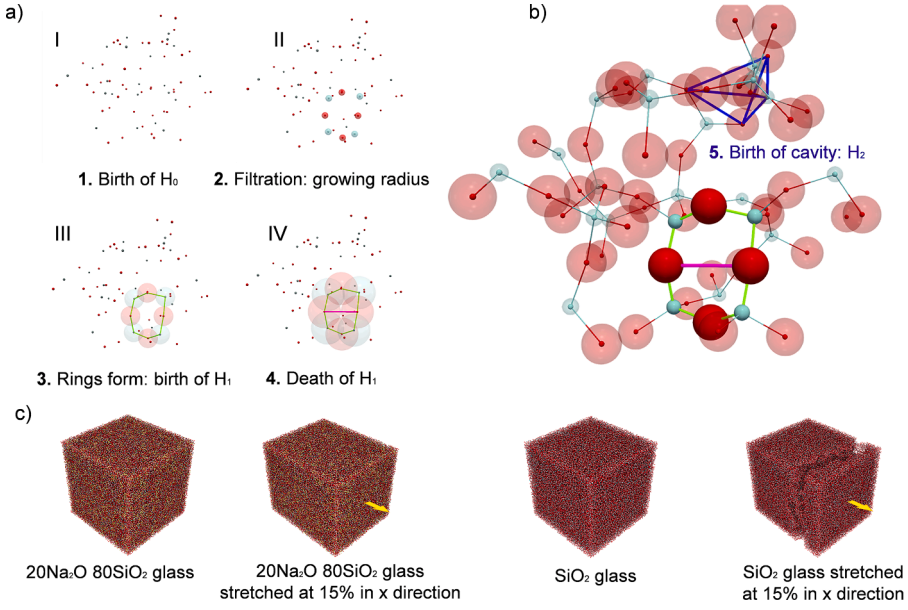

Fig. 1. Persistence diagram of vitreous SiO_2. In the depicted example, a glass cube of 1 nm x 1 nm x 1 nm was extracted from a structural model obtained through MD simulation at 300 K and using a strain rate of $\epsilon = 10^8 s^{-1}$ (see text for details; cyan: Si atoms, red: O atoms). The point coordinates of all atoms were used as the simplicial complex in persistent homology analysis. (a) Birth and death of one-dimensional simplices, H_1. (shown by way of example). (b) Birth and death of two-dimensional simplices, H_2 (denoted cavity). (c) Full MD models of sodium silicate and silica glasses before and after uniaxial stretching.

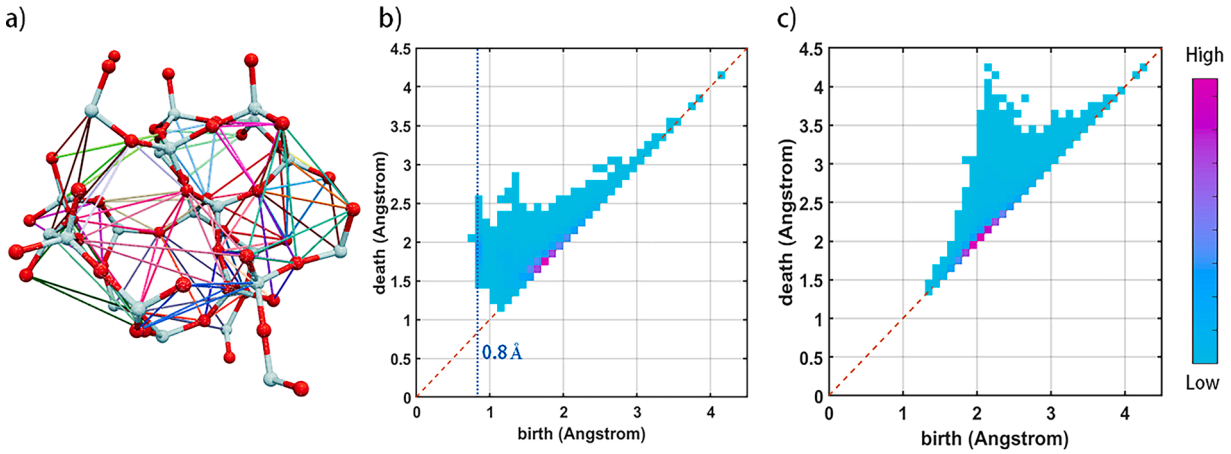

Fig. 2. (a) Structural representation of H_2 entities in a section of the simulated SiO_2 ensemble (cyan: Si atoms, red: O atoms). (b-c) Birth-death histograms (PDs) corresponding to H_1 and H_2.

The initial isotropic glasses were prepared by randomly placing 375.000 atoms according to the desired composition in a cubic periodic simulations box with an edge length that satisfies the experimental density for each composition [51]. Unrealistic overlaps between atoms were removed by running a short simulation at 5000 K for 1 ps while limiting the movement of atoms to 0.5 Å/step, with a step size of 1 fs. Next, the samples were equilibrated at 5000 K for 500 ps in the NVT (constant number of atoms, constant volume, constant temperature) ensemble. Then the samples were quenched linearly from 5000 K to room temperature (300 K) with a cooling rate of 1 K/ps while keeping the volume fixed. Finally, all glasses were further equilibrated at room temperature and zero pressure for 1 ns in the NPT (constant number of atoms, constant pressure, constant temperature) ensemble. The Nose-Hoover thermostat and barostat [52] were used for temperature and pressure control. The glass transition temperatures obtained using this model and for this cooling rate were 3000 K, 2700 K, 2510 K, 2350 K, and 2120 K, for silica and sodium silicate with increasing sodium content from 5 mol% to 20 mol%, respectively.

Radial distribution functions (RDF) and angular distribution functions for all pristine model ensembles are provided in **Fig. S1**. With a bond length of around 1.61 Å, the Si-O RDF is not affected by the Na_2O content. The Na-O RDF shows that the Na-O bond length slightly increases with increasing sodium content, i.e., from 2.267 Å to 2.317 Å. The O-Si-O angular distribution exhibits a well-defined peak centered around 108.5°, reflecting the tetrahedral short-range order. The angle between these tetrahedra is mainly captured by the Si-O-Si angular distribution function shown in **Fig. S1d**, with a broad distribution centered around 151° and slightly shifting towards smaller angles with increasing sodium content.

2.3. Deformation

The equilibrated stress-free isotropic glasses were subjected to tensile deformation along the *x*-direction at 300 K using a strain rate of 10^8 s^{-1}, while maintaining zero stress along the perpendicular directions. At strains of ϵ_d (where $\epsilon_d = 0$ %, 2.5 %, 5 %, 7.5 %, 10 %, 12.5 %, and 15 %), atomic structures were extracted for further topology analysis. Fig. 1**c** shows the atomic structure for $y = 0$ (silica) and $y = 0.2$ at 0 and 15 % strain. For the sample with $y = 0$, we observed critical failure at $\epsilon_d = 15$ %, however, none of the other MD samples broke when loaded to the same strain. The complete tensile stress-strain curves of all glasses are provided in **Fig. S2**, showing a very narrow plasticity regime (somewhat broadening with increasing sodium content), and an increase of the failure strain and a decrease of Young's modulus and yield stress with increasing sodium content.

2.4. Similarity analysis

The PD is a 2-dimensional histogram $\boldsymbol{A}$ ($I \times J$ matrix, indexing from 0 to $I - 1$ and J - 1). A grain interval of 0.1 Å was applied to count for birth and death datapoints. The same bounds of [0, 4.5] Å were set for both scales. The parameters i and j are the interval indices for birth and death, respectively. In order to compare the global PH of two glasses, we consider the similarity of their PDs. The similarity of any two such histograms is calculated from their cross-correlation normalized to their individual energies,

$$S = \max(\boldsymbol{s}(k,l)) = \max\left(\frac{\sum_{i=0}^{I-1}\sum_{j=0}^{J-1}\boldsymbol{A}_{i,j}\boldsymbol{B}_{i-k,j-l}}{\sqrt{\sum_{i=0}^{I-1}\sum_{j=0}^{J-1}\boldsymbol{A}_{i,j}^2 \cdot \sum_{i=0}^{I-1}\sum_{j=0}^{J-1}\boldsymbol{B}_{i,j}^2}}\right), \quad (1)$$

where $\boldsymbol{B}$ is the other histogram to compare to $\boldsymbol{A}$. The $\boldsymbol{s}$ is a 2I - 1 by 2 J - 1 matrix that evaluates the similarity of two histograms (images) by keeping $\boldsymbol{A}$ fixed and shifting $\boldsymbol{B}$ k rows upwards or downwards, or l columns to the left or right. The shifting indices k and l are within the ranges of [-I + 1, I-1] and [-J + 1, J-1], respectively. If the matrix $\boldsymbol{B}$ is indexed with row indices outside [0, I-1], or column indices outside [0, J-1], the concerning elements are padded with 0. The value of S denotes the degree of similarity, where a value of 1 indicates exactly identical PH, and a value of zero signifies no similarity at all.

3. Results and discussion

3.1. Compositional dependence of ring and cavity features

For isotropic $(Na_2O)_y$-$(SiO_2)_{1-y}$, the dependence of cumulative PH (summing-up over H_0, H_1, and H_2) on glass composition was previously reported by *Sørensen* et al. [53], using relatively small MD cells (3000 atoms). For studying possible statistical effects of structural anisotropy (as well as for generating anisotropy in the first place), we require larger models and, as will be shown in the following, deconvolution of H_1 and H_2. We will therefore focus our discussion on the global statistics in simulation cells involving 375 000 atoms, considering H_1 and H_2 features separately. We will start with the effect of chemical composition and focus on the subsequent similarity analysis and its application to the case of anisotropic glasses.

Fig. 2**b-c** show the PDs for the ring (H_1) and cavity (H_2) simplices in MD silica glass. The major part of the (global) structural information is concentrated alongside the diagonal (dashed line in Fig. 2**b-c**); only for H_1, there is a notable feature deviating from this line, born at around 0.8 Å. This feature resembles one-half of the fundamental Si-O interatomic distance; it is the shortest nodal distance in the model; therefore, the PD

is empty below this value for H_1 and H_2. Persistence (defined as the difference between birth and death) is zero on the diagonal and very small for the data accumulating alongside (<0.1 Å in the present case). Deviations from the diagonal (the widely scattering light-blue ranges in Figs. 2**b-c, S3, S5, S7, S9, S11, and S13**) are related to free volume within the network cavities (H_2), or within fundamental ring units (H_1). The absence of local maxima with finite persistence in H_2 indicates that cavity features are homogeneously arising from a fundamental distribution of ideal super-structural units (with low persistence and relatively high ionic packing density). For example, in H_2 of SiO_2, persistence extends to about 2.5 Å, meaning that the largest network cavities exhibit openings of ~ 0.5 nm beyond the effective ionic occupation of the network-forming atom species. The distinct persistent feature in H_1 (~ 0.8 Å) reflects smaller -Si-O-Si- rings, which are born around this length scale (in accordance with the Si-O bond length) and exhibit a persistence distribution peaking (opening length scale) at around 1.0 Å (death – birth); in this case, the persistence distribution contains information on the ring size distribution in these glasses [24].

In Fig. 3 and, further, in Supplementary Figures S3-S14, H_1 distributions are shown alongside the PD diagonals for the total of 35 datasets with variable chemical composition and degree of uniaxial strain, using the full set of atoms per model (including oxygen) as well as for the individual Si and Na graphs, respectively. We have two qualitative reference scales to evaluate these distributions, *i.e.*, the mean Si-O bond length (see above) and the typical distance between a sodium ion and its charge-compensating non-bridging oxygen opponent, Na^+–NBO^-. For linear Si-O-Si and Na-O-Na bridges, birth events would appear at these length values in the PD of the pure Si and Na graphs, respectively (and similarly, at half of these lengths when including oxygen atoms). Since the structural linkages are not linear in the actual glass models, the reference values represent upper bounds for next-neighbor interactions. The PD data indicate that the overall effect of increasing the Na_2O concentration is the appearance of rings at around 1.6 Å, while larger rings are consumed compared to pure SiO_2 (black curve in Fig. 3a). H_1 of the Si skeleton alone does not vary significantly, except for some ring dilation, probably in response to accommodating Na species (Fig. 3b). Very similarly, this is also seen in the H_2 distribution of the Si skeleton (Fig. 3e), where a new cavity mode grows in at around 3.3 Å (we may speculate that these are Si skeleton cavities within which multiple Na ions are incorporated at the same time, as discussed in the following). The H_1 distribution of the Na atoms alone indicates that they are initially (at low concentration, $y = 0.05$) incorporated randomly, with a mean Na-Na distance of ~ 10 Å (corresponding to a Na ion density of ~ 10^{21} cm^{-3}, in good agreement with the experimental molar volume of the glass at this sodium ion concentration, see Fig. 3c). At higher Na content, the ring and cavity sizes do not only become significantly smaller, but the H_1 distribution also evolves from more random to highly correlated, with a peak near 2 Å (below the linear Na^+-NBO^- - Na^+-distance) and another one near 3.3 Å. H_2 observations corroborate these H_1 interpretations (Fig. 3f), except that there are fewer cavity features involving direct Na-O-Na interaction born near 2 Å (probably because Na triclusters are much less frequent).

Overall, adding Na leads to the creation of more and smaller rings and cavities (Fig. 3**a** and **d**), with Na being less and less randomly distributed (Fig. 3**c**). In particular, the number of H_1 features with a characteristic scale close to that of the Na^+-NBO^- bridge indicates preferential clustering (Fig. 3**c**). Interestingly, the increase in the fraction of smaller rings is not accompanied by a similarly strong increase in the occurrence of the smallest cavities (Fig. 3**f**). From this observation, we conclude that the Na-O cluster size is limited to 2–3 Na ions, *i.e.*, not sufficient to reflect in H_2 features in the Na skeleton. In the Si skeleton, the ring and cavity distributions shift the balance in favor of larger features: the frequency of those features which are already larger than the Na^+-NBO^- bridge increases further; it is unlikely for a Na^+ ion to

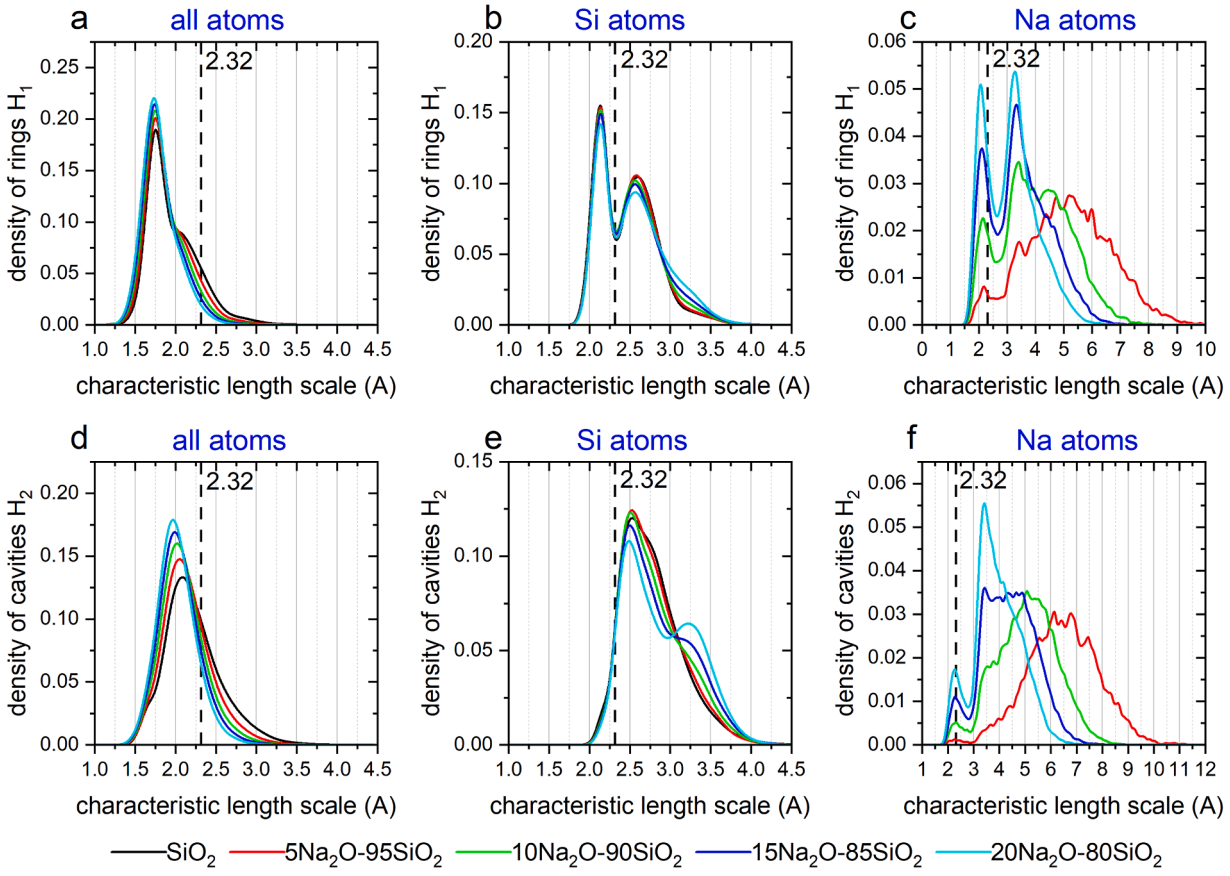

Fig. 3. Density distribution of H_1 (a-c) and H_2 (d-f) entities for graph representations including all atoms, only Si or only Na. All plots are at 0 % strain.

widen any interstices that are too small to accommodate the modifier in the first place (Fig. 3**b** and **e**). The parallel evolutions of the Na and the Si skeletons indicate that Na accumulates within the larger H_2 features seen on the Si network; the existence of larger backbone cavities is the most probable reason for the selective precipitation of Na once a concentration threshold is reached: Na preferably accumulates in network voids, leading to non-random topology.

3.2. *Effects of uniaxial strain*

At first view, there is only very little variation in PDs of isotropic versus anisotropic glasses of similar chemical composition (see **Fig. S3**). This is expected because structural anisotropy in glasses is often assumed to be an entropic [28], fully reversible [54,55] effect of delayed or frozen-in elasticity [56]. Topological analyses, on the other hand, would be sensitive only to network variations, requiring (directional) bond-switching reactions leading to variations in the ring and cavity size distributions.

For a detailed view, similarity analyses were conducted on the global H_1 and H_2 distributions, for the full set of atoms as well as for the individual Si and Na graphs (Fig. 4). From this analysis, we find weak but systematic variations in PH induced by anisotropic strain. These variations depend on chemical composition and the extent of strain and affect the Si and the Na graphs differently. In general and except for the Si graph, the statistical variation between PDs before and after stretching is on the order of 1 % (Eq. (1)); it reaches 6 % when considering the Si backbone alone (note that the datapoint for 15 % strain in all atoms/silica-only PDs is a result of network rupture, see Fig. 1**c**). Higher Na concentration reduces the PD dissimilarity caused by anisotropic strain, and there seems to be a systematic maximum in dissimilarity at a strain of around 12 %. The data shown in Fig. 4 indicate that topological variations induced by anisotropic stretching occur primarily in the ring structure of the Si-O-Si network backbone. Cavity features (H_2) are much less affected. This seems to describe a type of deformation where the cavity volume is retained; anisotropic stretching appears to be governed by shear deformation of the SiO4 skeleton. After fracture (SiO_2 with $\varepsilon_d = 15$ %), similarity is recovered.

4. Conclusion

We analyzed persistent homology of SiO_2–Na_2O MD glass ensembles with variable alkali concentration as a function of frozen-in anisotropic strain. Statistical information was extracted on ring (H_1) and cavity (H_2) features, whereby anisotropic stretching was found to induce strong variations in the ring topology of the –O-Si-O- backbone, but only minor changes in the overall cavity statistics or in the Na distribution (whereby the Na distribution was found to be directly related to H_2 cavity statistics of the –O-Si-O- backbone, with direct Na-Na interactions being governed by H_2 cavity persistence). Tensile fracture was found to lead to total recovery of network topology relative to the pristine (isotropic) glass.

CRediT authorship contribution statement

Zhiwen Pan: Writing – original draft, Visualization, Validation, Methodology, Investigation, Formal analysis. **Achraf Atila:** Writing – review & editing, Visualization, Validation, Investigation, Data curation. **Erik Bitzek:** Writing – review & editing, Validation, Supervision, Funding acquisition. **Lothar Wondraczek:** Writing – review & editing, Writing – original draft, Validation, Supervision, Methodology, Funding acquisition, Conceptualization.

Declaration of competing interest

The authors declare that they have no known competing financial interests or personal relationships that could have appeared to influence the work reported in this paper.

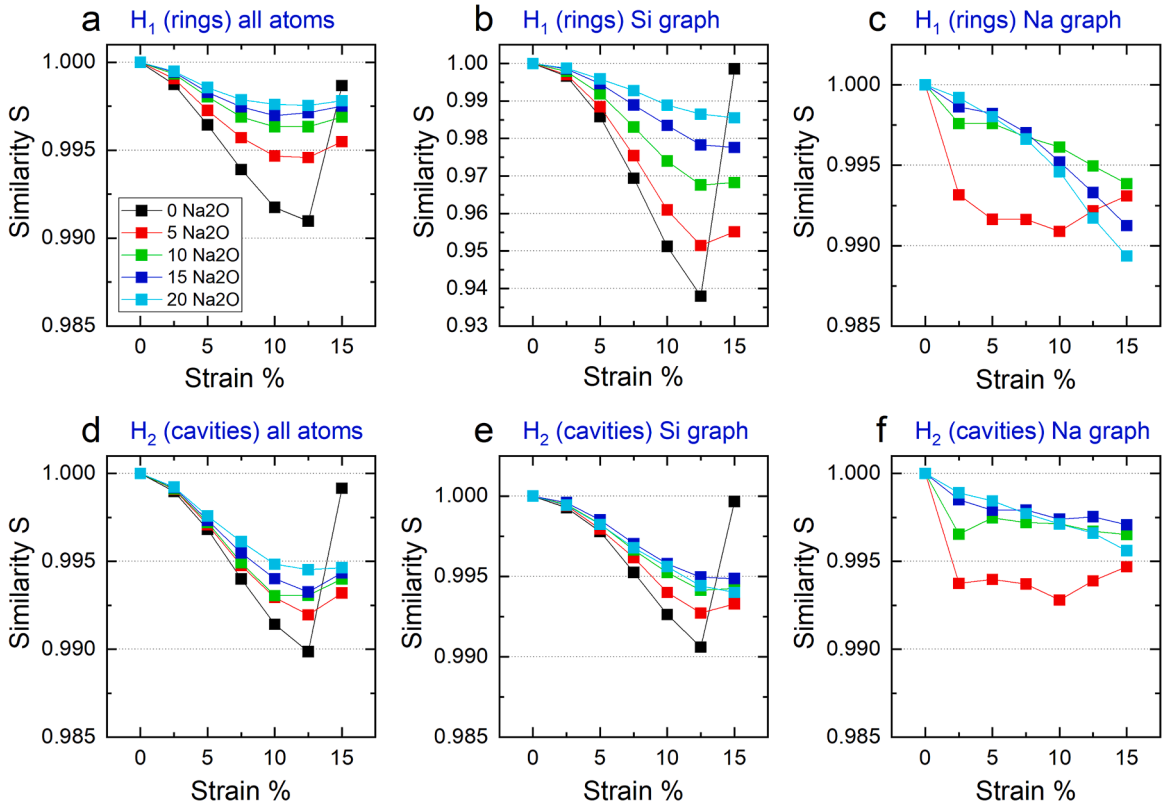

Fig. 4. Variation of H_1 (a-c) and H_2 (d-f) after stretching, expressed as the change in PD similarity relative to the pristine ($\varepsilon_d = 0$ %) MD ensemble.

Data availability

Data will be made available on request.

Acknowledgements

We gratefully acknowledge funding of this work by the German Research Foundations within its priority programs SPP 2315 (Hetero-aggregates) and SPP1594 (Topological Engineering of Ultrastrong Glasses).

Supplementary materials

Supplementary material associated with this article can be found, in the online version, at doi:10.1016/j.jnoncrysol.2023.122801.

References

[1] W. Vogel, Glass Chemistry, Springer Berlin Heidelberg, 1994.
[2] G.S. Henderson, J.F. Stebbins, The short-range order (SRO) and structure, Rev. Mineral. Geochem. 87 (2022) 1–53, https://doi.org/10.2138/RMG.2022.87.01.
[3] J.W.E. Drewitt, L. Hennet, D.R. Neuville, From short to medium range order in glasses and melts by diffraction and Raman spectroscopy, Rev. Mineral. Geochem. 87 (2022) 55–103, https://doi.org/10.2138/RMG.2022.87.02.
[4] C. Calahoo, L. Wondraczek, Ionic glasses: structure, properties and classification, J. Non-Cryst. Solids 8 (2020), https://doi.org/10.1016/j.nocx.2020.100054.
[5] J.C. Phillips, Topology of covalent non-crystalline solids I: short-range order in chalcogenide alloys, J. Non Cryst. Solids 34 (1979) 153–181, https://doi.org/10.1016/0022-3093(79)90033-4.
[6] T. Aste, M. Saadatfar, T.J. Senden, Geometrical structure of disordered sphere packings, Phys. Rev. E Stat. Nonlin. Soft Matter Phys. 71 (2005) 061302, https://doi.org/10.1103/PHYSREVE.71.061302.
[7] P.K. Gupta, J.C. Mauro, Composition dependence of glass transition temperature and fragility. I. A topological model incorporating temperature-dependent constraints, J. Chem. Phys. 130 (2009) 094503, https://doi.org/10.1063/1.3077168.
[8] M.M. Smedskjaer, J.C. Mauro, S. Sen, Y. Yue, Quantitative design of glassy materials using temperature-dependent constraint theory, Chem. Mater. 22 (2010) 5358–5365, https://doi.org/10.1021/CM1016799.
[9] L. Wondraczek, J.C. Mauro, J. Eckert, U. Kühn, J. Horbach, J. Deubener, T. Rouxel, L. Wondraczek, J.C. Mauro, J. Eckert, U. Kühn, J. Horbach, J. Deubener, T. Rouxel, Towards ultrastrong glasses, Adv. Mater. 23 (2011) 4578–4586, https://doi.org/10.1002/ADMA.201102795.
[10] J.C. Mauro, Topological constraint theory of glass, Am. Ceram. Soc. Bull. 90 (2020) (n.d.).
[11] Y. Hiraoka, T. Nakamura, A. Hirata, E.G. Escolar, K. Matsue, Y. Nishiura, Hierarchical structures of amorphous solids characterized by persistent homology, Proc. Natl. Acad. Sci. USA. 113 (2016) 7035–7040, https://doi.org/10.1073/PNAS.1520877113.
[12] Z. Pan, J. Dellith, L. Wondraczek, Genome mining in glass chemistry using linear component analysis of ion conductivity data, Adv. Sci. 10 (2023) 2301435, https://doi.org/10.1002/ADVS.202301435.
[13] K.A. Kirchner, D.R. Cassar, E.D. Zanotto, M. Ono, S.H. Kim, K. Doss, M.L. Bødker, M.M. Smedskjaer, S. Kohara, L. Tang, M. Bauchy, C.J. Wilkinson, Y. Yang, R. S. Welch, M. Mancini, J.C. Mauro, Beyond the average: spatial and temporal fluctuations in oxide glass-forming systems, Chem. Rev. (2021), https://doi.org/10.1021/ACS.CHEMREV.1C00974.
[14] Z. Pan, O. Benzine, S. Sawamura, R. Limbach, A. Koike, T.D. Bennett, G. Wilde, W. Schirmacher, L. Wondraczek, Disorder classification of the vibrational spectra of modern glasses, Phys. Rev. B 104 (2021), https://doi.org/10.1103/PHYSREVB.104.134106.
[15] B.P. Rodrigues, J.C. Mauro, Y. Yue, L. Wondraczek, Modifier constraints in alkali ultraphosphate glasses, J. Non Cryst. Solids 405 (2014) 12–15, https://doi.org/10.1016/J.JNONCRYSOL.2014.08.035.
[16] C. Hermansen, B.P. Rodrigues, L. Wondraczek, Y. Yue, An extended topological model for binary phosphate glasses, J. Chem. Phys. 141 (2014) 244502, https://doi.org/10.1063/1.4904287.
[17] B.P. Rodrigues, L. Wondraczek, Medium-range topological constraints in binary phosphate glasses, J. Chem. Phys. 138 (2013) 244507, https://doi.org/10.1063/1.4810868.
[18] N. Otter, M.A. Porter, U. Tillmann, P. Grindrod, H.A. Harrington, A roadmap for the computation of persistent homology, EPJ Data Sci. 6 (2017), https://doi.org/10.1140/EPJDS/S13688-017-0109-5.
[19] A. Zomorodian, G. Carlsson, Computing persistent homology, Discrete. Comput. Geom. 33 (2005) 249–274, https://doi.org/10.1007/S00454-004-1146-Y.
[20] Y. Onodera, Y. Takimoto, H. Hijiya, T. Taniguchi, S. Urata, S. Inaba, S. Fujita, I. Obayashi, Y. Hiraoka, S. Kohara, Origin of the mixed alkali effect in silicate glass, NPG Asia Mater. 11 (2019), https://doi.org/10.1038/S41427-019-0180-4.
[21] T. Shirai, T. Nakamura, Microscopic description of yielding in glass based on persistent homology, J. Phys. Soc. Jpn. 88 (2019), https://doi.org/10.7566/JPSJ.88.074801.
[22] Y. Onodera, S. Kohara, S. Tahara, A. Masuno, H. Inoue, M. Shiga, A. Hirata, K. Tsuchiya, Y. Hiraoka, I. Obayashi, K. Ohara, A. Mizuno, O. Sakata, Understanding diffraction patterns of glassy, liquid and amorphous materials via persistent homology analyses, J. Ceram. Soc. Jpn. 127 (2019) 853–863, https://doi.org/10.2109/JCERSJ2.19143.
[23] T. Nakamura, Y. Hiraoka, A. Hirata, E.G. Escolar, Y. Nishiura, Persistent homology and many-body atomic structure for medium-range order in the glass, Nanotechnology 26 (2015), https://doi.org/10.1088/0957-4484/26/30/304001.
[24] S.S. Sørensen, T. Du, C.A.N. Biscio, L. Fajstrup, M.M. Smedskjaer, Persistent homology: a tool to understand medium-range order glass structure, J. Non-Cryst. Solids 16 (2022) 100123, https://doi.org/10.1016/J.NOCX.2022.100123.
[25] H. Stockhorst, R. Brückner, Structure sensitive measurements on phosphate glass fibers, J. Non Cryst. Solids 85 (1986) 105–126, https://doi.org/10.1016/0022-3093(86)90083-9.
[26] Y. Yue, R. Brückner, Comparison of some non-Newtonian flow equations for inorganic glass melts and amorphous polymers, J. Non Cryst. Solids 202 (1996) 253–265, https://doi.org/10.1016/0022-3093(96)00188-3.
[27] X. Yang, G. Scannell, C. Jain, B.P. Rodrigues, M.A. Schmidt, L. Wondraczek, Permanent structural anisotropy in a hybrid fiber optical waveguide, Appl. Phys. Lett. 111 (2017) 201901, https://doi.org/10.1063/1.4999048.
[28] S. Inaba, H. Hosono, S. Ito, Entropic shrinkage of an oxide glass, Nat. Mater. 14 (2014) 312–317, https://doi.org/10.1038/nmat4151, 2014 14:3.
[29] J. Deubener, L. Wondraczek, Anisotropic alkali silicate glasses by frozen-in strain, Ceram. Trans. 170 (2005) 47–56, https://doi.org/10.1002/9781118408063.CH4.
[30] S. Wang, C. Jain, L. Wondraczek, K. Wondraczek, J. Kobelke, J. Troles, C. Caillaud, M.A. Schmidt, Non-Newtonian flow of an ultralow-melting chalcogenide liquid in strongly confined geometry, Appl. Phys. Lett. 106 (2015) 201908, https://doi.org/10.1063/1.4921708.
[31] W. Zhu, M.A.T. Marple, B.G. Aitken, S. Sen, Universality in the non-Newtonian viscous flow behavior of AsxSe1 − x liquids: results from capillary rheometry, J. Non Cryst. Solids 453 (2016) 42–45, https://doi.org/10.1016/J.JNONCRYSOL.2016.09.019.
[32] B.P. Rodrigues, T. To, M.M. Smedskjaer, L. Wondraczek, Mechanical properties of oxide glasses, Rev. Mineral. Geochem. 87 (2022) 229–281, https://doi.org/10.2138/RMG.2022.87.06.
[33] S. Ganisetti, A. Atila, J. Guénolé, A. Prakash, J. Horbach, L. Wondraczek, E. Bitzek, The origin of deformation induced topological anisotropy in silica glass, Acta Mater. 257 (2023) 119108, https://doi.org/10.1016/J.ACTAMAT.2023.119108.
[34] L. Wondraczek, E. Bouchbinder, A. Ehrlicher, J.C. Mauro, R. Sajzew, M. M. Smedskjaer, Advancing the mechanical performance of glasses: perspectives and challenges, Adv. Mater. 34 (2022) 2109029, https://doi.org/10.1002/ADMA.202109029.
[35] B. Kusz, K. Trzebiatowski, R.J. Barczynski, Ionic conductivity of bismuth silicate and bismuth germanate glasses, Solid State Ion. 159 (2003) 293–299, https://doi.org/10.1016/S0167-2738(02)00911-6.
[36] A. Paraskiva, M. Bokova, E. Bychkov, Na+ ion conducting glasses in the NaCl-Ga2S3-GeS2 system: a critical percolation regime, Solid State Ion. 299 (2017) 2–7, https://doi.org/10.1016/J.SSI.2016.11.003.
[37] A. Bunde, Application of percolation theory in composites and glasses, Solid State Ion 75 (1995) 147–155, https://doi.org/10.1016/0167-2738(94)00146-J.
[38] G.N. Greaves, EXAFS and the structure of glass, J. Non Cryst. Solids 71 (1985) 203–217, https://doi.org/10.1016/0022-3093(85)90289-3.
[39] I. Obayashi, HomCloud, (n.d.). https://homcloud.dev/index.en.html.
[40] I. Obayashi, T. Nakamura, Y. Hiraoka, Persistent homology analysis for materials research and persistent homology software: HomCloud, Https://Doi.Org/10.7566/JPSJ.91.091013. 91 (2022). https://doi.org/10.7566/JPSJ.91.091013.
[41] R. Diestel, Graphs and their representation, Graph Theory 173 (2017) 1–12.
[42] A.P. Thompson, H.M. Aktulga, R. Berger, D.S. Bolintineanu, W.M. Brown, P. S. Crozier, P.J. in 't Veld, A. Kohlmeyer, S.G. Moore, T.D. Nguyen, R. Shan, M. J. Stevens, J. Tranchida, C. Trott, S.J. Plimpton, LAMMPS - a flexible simulation tool for particle-based materials modeling at the atomic, meso, and continuum scales, Comput. Phys. Commun. 271 (2022) 108171, https://doi.org/10.1016/j.cpc.2021.108171.
[43] A. Pedone, G. Malavasi, M. Cristina Menziani, A.N. Cormack, U. Segre, A new self-consistent empirical interatomic potential model for oxides, silicates, and silica-based glasses, J. Phys. Chem. B 110 (2006) 11780–11795, https://doi.org/10.1021/jp0611018.
[44] B. Deng, J. Luo, J.T. Harris, C.M. Smith, T.M. Wilkinson, Toward revealing full atomic picture of nanoindentation deformation mechanisms in Li2O-2SiO2 glass-ceramics, Acta Mater. 208 (2021) 116715, https://doi.org/10.1016/J.ACTAMAT.2021.116715.
[45] J. Luo, B. Deng, K.D. Vargheese, A. Tandia, S.E. DeMartino, J.C. Mauro, Atomic-scale modeling of crack branching in oxide glass, Acta Mater. 216 (2021) 117098, https://doi.org/10.1016/J.ACTAMAT.2021.117098.
[46] B. Deng, J. Luo, J.T. Harris, C.M. Smith, M.E. McKenzie, Molecular dynamics simulations on fracture toughness of Al2O3-SiO2 glass-ceramics, Scr. Mater. 162 (2019) 277–280, https://doi.org/10.1016/J.SCRIPTAMAT.2018.11.034.
[47] A. Atila, Y. Ouldhnini, S. Ouaskit, A. Hasnaoui, Atomistic insights into the mixed-alkali effect in phosphosilicate glasses, Phys. Rev. B 105 (2022) 134101, https://doi.org/10.1103/PHYSREVB.105.134101.
[48] A. Atila, S. Ouaskit, A. Hasnaoui, Ionic self-diffusion and the glass transition anomaly in aluminosilicates, Phys. Chem. Chem. Phys. 22 (2020) 17205–17212, https://doi.org/10.1039/D0CP02910F.

[49] A. Atila, E.M. Ghardi, S. Ouaskit, A. Hasnaoui, Atomistic insights into the impact of charge balancing cations on the structure and properties of aluminosilicate glasses, Phys. Rev. B 100 (2019), https://doi.org/10.1103/PHYSREVB.100.144109.
[50] C.J. Fennell, J.D. Gezelter, Is the Ewald summation still necessary? Pairwise alternatives to the accepted standard for long-range electrostatics, J. Chem. Phys. 124 (2006) 234104, https://doi.org/10.1063/1.2206581.
[51] Y. Vaills, Y. Luspin, G. Hauret, Two opposite effects of sodium on elastic constants of silicate binary glasses, Mater. Sci. Eng. 40 (1996) 199–202, https://doi.org/10.1016/0921-5107(96)01604-2.
[52] W. Shinoda, M. Shiga, M. Mikami, Rapid estimation of elastic constants by molecular dynamics simulation under constant stress, Phys. Rev. B 69 (2004) 134103, https://doi.org/10.1103/PhysRevB.69.134103.
[53] S.S. Sørensen, C.A.N. Biscio, M. Bauchy, L. Fajstrup, M.M. Smedskjaer, Revealing hidden medium-range order in amorphous materials using topological data analysis, Sci. Adv. 6 (2020), https://doi.org/10.1126/SCIADV.ABC2320.
[54] B. Martin, L. Wondraczek, J. Deubener, Y. Yue, Mechanically induced excess enthalpy in inorganic glasses, Appl. Phys. Lett. 86 (2005) 121917, https://doi.org/10.1063/1.1895483.
[55] J. Endo, S. Inaba, S. Ito, Relaxation of anisotropic alkali metaphosphate glass, Mater. Lett. 283 (2021) 128762, https://doi.org/10.1016/J.MATLET.2020.128762.
[56] A.S. Argon, Delayed elasticity in inorganic glasses, J. Appl. Phys. 39 (1968) 4080, https://doi.org/10.1063/1.1656927.